Electrochimica Acta 502 (2024) 144819

Contents lists available at ScienceDirect

Electrochimica Acta

journal homepage: www.journals.elsevier.com/electrochimica-acta

Comparative electrochemical and thermodynamic study of cold-rolled steel, Al alloy AA5754, and Zn corrosion in fluoride and chloride solutions

Ana Kraš [a,b], Ingrid Milošev [a,c,*]

[a] Department of Physical and Organic Chemistry, Jožef Stefan Institute, Jamova c. 39, Ljubljana 1000, Slovenia
[b] Jožef Stefan Postgraduate School, Jamova c. 39, Ljubljana SI-1000, Slovenia
[c] Valdoltra Orthopaedic Hospital, Jadranska c. 31, Ankaran SI-6280, Slovenia

ARTICLE INFO

Keywords:
Equilibrium calculations
Pourbaix diagrams
E-pH diagrams
Specific ion interaction theory
Fluoride
Chloride
Cold-rolled steel
Aluminium alloy
Zinc
Ammonium
Bicarbonate
Pitting
Complexation

ABSTRACT

This study investigates the effects of fluoride and chloride ions on the corrosion of cold-rolled steel, aluminium alloy AA5754, and zinc, using ammonium bicarbonate as a buffer at pH 4 and compares electrochemical findings with thermodynamic calculations of *E*-pH diagrams. The distinct electrochemical behaviours of fluoride and chloride ions were confirmed, with fluoride-induced corrosion leading to the significant complex formation on cold-rolled steel and AA5754, the latter leading to a narrowing of the Al passive region. However, a comprehensive analysis of all ionic species in the solution (F^-, Cl^-, NH_4^+ and HCO_3^-) and their complex equilibria reveals that zinc's corrosion is primarily influenced by the overall ionic strength of the solution and further complexation with the buffering agent at higher pH levels, should these conditions occur during corrosion. In addition, this analysis also highlights the subtle differences in the stabilization effects of open circuit potential on cold-rolled steel and AA5754. The results underscore the importance of considering the overall solution equilibrium in thermodynamic analyses and provide a foundation for further research on the role of F^- and Cl^- ions in zirconium conversion coatings.

1. Introduction

The behaviour of halide ions such as fluoride and chloride ions deserves attention in corrosion research due to their potentially detrimental effect on the dissolution and passivity of various metals. In acidic solutions containing F^-, passive films on Fe were shown to dissolve uniformly due to the increased stability of HF complexes with surface Fe cations in more acidic environments, while at pH > 5, pitting corrosion occurs [1,2]. This was ascribed to decreased formation and transfer of soluble F-complexes, leading to less pronounced oxide layer thinning and localized attack in less acidic to basic conditions [1,3]. For chlorides, it was observed that Cl-induced pitting on Fe occurs above a critical Cl^- concentration $c = 0.3$ mM and below a critical pH = 10.4 [4].

It is widely recognised that fluoride ions can effectively remove aluminium oxide films by forming aluminium-fluoride complexes and soluble AlF_3 films [5–7]; this process is essential in conversion coating solutions [8]. In contrast, Cl^- ions initiate a more localised attack in the form of pitting [5,6,9–11]. Similarly, it was demonstrated that Cl^- ions enhance corrosion by promoting the breakdown of air-formed oxide films and by assisting in maintaining an aggressive pitting microenvironment on carbon steel [12].

Xue et al. [7] found that in H_2SO_4 solutions with F^- ions, aluminium forms various Al–*F* complexes, influenced by fluoride concentration and solution pH, while zinc and iron remain unaffected by fluoride. This was further supported by the construction of *E*-pH (Pourbaix) diagrams.

The presence of Cl^- ions in F^- solutions further complicates this interaction, with studies by Carroll et al. [11] demonstrating that fluoride ions can modify aluminium oxide surfaces within specific concentration ranges, increasing susceptibility to Cl-induced corrosion. On the other hand, the study by Trompette et al. [13] offered a refined perspective by proposing that the corrosiveness of halide ions, including fluoride and chloride, should be evaluated beyond their ionic size, focusing instead on their interactions with water molecules. In particular, F^- ions (at pH=8.1), acting as cosmotropes, form robust bonds with water, thereby stabilising its structure and mitigating corrosion by preserving their hydration shells. In contrast, Cl^- ions (at pH = 6.6), characterised as chaotropic, weaken water's structural integrity, making it easier to dehydrate and infiltrate metal oxides, thus promoting pitting

* Corresponding author at: Department of Physical and Organic Chemistry, Jožef Stefan Institute, Jamova c. 39, Ljubljana 1000, Slovenia.
E-mail address: ingrid.milosev@ijs.si (I. Milošev).

https://doi.org/10.1016/j.electacta.2024.144819
Received 1 April 2024; Received in revised form 6 July 2024; Accepted 1 August 2024
Available online 2 August 2024

corrosion on Al. This was further observed on Fe in alkaline solutions (pH=10), where the kinetics of F^- attack were significantly lower than Cl^- [14]. Summarising these studies, it can be stated that the effect of fluoride and chloride ions was fundamentally studied more on aluminium and its alloys [5–11,13,15–18] and, to a lesser extent, on iron/carbon steel [1–4,7,12,14,19] and zinc substrates [20–23]. Moreover, it seems like the vast majority of newer literature data dealt with halide ions in terms of the type of electrolyte and not focusing on the fundamental aspect of their influence on different substrates.

In the realm of conversion coatings, particularly zirconium conversion coatings (ZrCCs), which present an environmentally friendly alternative to chromate and phosphate coatings, various additives to conversion baths have been employed for ZrCC modification [24]. The observed corrosion aggressiveness of fluoride ions is used in the context of ZrCCs as it leads to surface activation of aluminium by removal of the native film, thus priming it for more uniform ZrCC deposition. Concurrently, the less aggressive ZrF_6^{2-} ions, otherwise the primary Zr-bearing component, improve the surface's wettability for the successful deposition of subsequent layers [25]. In addition, fluoride complexation with ZrF_6^{2-} uniquely extends the ZrCC operational window by delaying the onset of Zr hydrolysis and precipitation to more manageable pH levels, as shown in our previous work [26]. Nevertheless, it was also indicated that ZrF_6^{2-} has an etching effect, albeit at high concentrations (10^{-2}–10^{-1} M [27,28]).

In contrast to fluoride, chloride ions are not so commonly used as additives in conversion coating baths. However, there are some instances of providing titanium conversion coatings, which are similar to ZrCCs, with chloride sources like $TiCl_4$ [29–33]. Nevertheless, it is difficult to apprehend how this is accomplished, considering the vigorous nature of $TiCl_4$ [34]. Additionally, ZrCC baths often include ammonium bicarbonate as a pH adjuster and buffer, highlighting the complex interplay of various additives in corrosion processes. Given all this intricate interaction, a nuanced understanding of the individual and combined effects of fluoride and chloride ions on different substrates and in the presence of other solution additives is essential.

Building upon literature research of exploration of ZrCC bath parameters across various substrates [35,36], including aluminium and its alloys [37–39], cold-rolled steel (CRS) [40,41], and zinc [42,43]; with a comprehensive review of ZrCC behaviour on different substrates, including the aforementioned references and more, provided in [24], our initial goal was to compare the effects of free fluoride and chloride ions on the corrosion of the three substrates at pH 4. Our previous study showed that pH around 4 is the most significant for ZrCC deposition [26]. Although ZrF_6^{2-} species are essential for the deposition of ZrCC, we deliberately excluded ZrF_6^{2-} these species in the present study and focused on the role of fluoride. Namely, it was reported that ZrF_6^{2-} is not involved in the process of thinning or removal of the native oxide layer on Al alloy; instead, this role has free F^-, while ZrF_6^{2-}, due to its mild nature' rather leads to an increase in hydrophilicity [25]. The effect of Cl^- in the conversion bath is similar to that of F^- but markedly less aggressive [44]. When in contact with HCl and HF acids, the dissolution of Al results in the formation of $AlCl_3$ and AlF_3. The latter is much more soluble, resulting in a continuous dissolution of Al. The larger solubility of AlF_3 is related to its typical ionic character, whereas $AlCl_3$ and other Al halides also express covalent character of the bonding, resulting in a lower solubility [34].

Our experimental endeavour has expanded into detailed equilibrium calculations considering the solution composition, including the buffering agent and ion interactions in much more complex equilibria. To the best of our knowledge, no study has yet investigated the combined effects of fluoride and chloride solutions with ammonium bicarbonate on these particular substrates. In our opinion, this approach highlights the importance of evaluating all species present in the solution at their respective concentrations and lays a foundational framework for future corrosion studies involving complex solutions, particularly those incorporating conversion agents and additives in conversion coating baths.

2. Experimental section

2.1. Materials

Low-carbon cold-rolled steel (CRS) panels, 1 mm thick from ACT Test Panels LLC, Hillsdale, Michigan, USA, had a chemical composition determined by X-ray fluorescence spectroscopy: C 0.0420 wt.%, Mn 0.2 wt.%, S 0.01 wt.%, Fe remainder. Zinc, in 1 mm thick foils from Goodfellow Cambridge Ltd., U.K., had a specified composition of 98.8% Zn. Aluminium alloy EN AW−5754 (AA5754), 1.5 mm thick panels from Impol 2000 dd., Slovenska Bistrica, Slovenia, had a specified composition: Mg 2.6–3.6 wt.%, Mn 0–0.5 wt.%, Si 0–0.4 wt.%, Fe 0–0.4 wt.%, Cr 0–0.3 wt.%, Zn 0–0.2 wt.%, Ti 0–0.15 wt.%, Cu 0–0.1 wt.%, Al remainder. Original panels were cut into 2.5 cm × 3.5 cm square sheet specimens with 3 mm diameter holes for immersion into solution.

2.2. Chemicals

Solutions used in this work were prepared from as received analytical reagent grade chemicals: absolute ethanol (EtOH, Merck KGaA, Darmstadt, Germany), HF (39.5%, Carlo Erba, Val de Reuil Cedex, France), HCl (37%, VWR International S.A.S, Fontenay−sous−Bois, France) and NH_4HCO_3 (Sigma−Aldrich, Steinheim, Germany). For chemical pre-treatments, SurTec®'s chemical products (SurTec International GmbH, Bensheim, Germany), supplied by SurTec Adria, d.o.o. (Ljubljana, Slovenia) were used: SurTec® 089, SurTec® 132, SurTec® 141 and SurTec® 496. The solutions were prepared utilising Milli-Q Direct water (Millipore, Billerica, Massachusetts, USA) with a resistivity of 18.2 MΩ cm at 25 °C, ensuring a total organic carbon (TOC) value below 5 ppb for rinsing samples and solution formulation.

2.3. Samples and pre-treatment

2.3.1. Grinding

Sample preparation commenced with manually wet-grinding on a LaboPol−5 machine at 300 rpm, using SiC papers up to a P4000 grit, supplied by Struers (Ballerup, Denmark). Post-grinding, the samples were subjected to a 5 min ultrasonic cleaning in absolute ethanol, using an Elmasonic P bath at 37 kHz and full power. In the end, samples were rinsed in absolute ethanol and Milli-Q water and dried using compressed nitrogen.

2.3.2. Chemical pre-treatment

The chemical pre-treatment step removes impurities and ensures a hydrophilic surface for the subsequent conversion [25]. Glass beakers with a volume of 500 mL were employed for the rinsing baths. The chemical treatment process for all substrates involved alkaline cleaning and an additional desmutting step for AA5754 using SurTec® solutions, conducted on a C−MAG HS 7 magnetic hotplate stirrer (IKA®−Werke GmbH & Co. KG, Staufen, Germany) with stirring at 150 rpm and a temperature of 60 °C, except for the desmutting phase, which occurred at room temperature. This was carried out following lab-adapted recommendations from SurTec®, tailored to each substrate:

For CRS: An alkaline cleaning for 5 min using a solution composed of 5 vol.% (50 mL/L) SurTec® 132 [45] and 0.6 vol.% (6 mL/L) SurTec® 089 [46], with a pH of 7.3.

For AA5754: An alkaline cleaning for 10 min using a solution containing 3 vol.% (30 mL/L) SurTec® 132 [45] and 0.5 vol.% (5 mL/L) SurTec® 089 [46], with a pH of 7.4, followed by an acid desmutting for 3 min using a solution of 20 vol.% (200 mL/L) SurTec® 496 [47], with a pH of 0.3.

For Zn: An alkaline cleaning for 5 min using a mixture of 2 vol.% (20 mL/L) SurTec® 141 [48] and 0.5 vol.% (5 mL/L) SurTec® 089 [46], with a pH of 12.8.

Each alkaline cleaning/desmutting step was followed by a double rinse with Milli-Q Direct water: (i) ca. 30 s rigorous circular rinse with a

wash bottle on both sample sides, and (ii) a 1 min dip in a clean Milli-Q Direct water bath. More details will be available in our forthcoming studies.

2.4. Electrochemical measurements

Electrochemical experiments were carried out with a Multi Autolab/M204 (Metrohm Autolab, Utrecht, Netherlands) potentiostat/galvanostat controlled by Nova 2.1. software. Measurements were conducted in homemade modified "clamp-on" electrochemical cells (250 mL), suitable for flat, thin-coated samples and less susceptible to crevice corrosion [49]. Electrochemical measurements were performed in a three−compartment set-up: the sample as a working electrode (WE) was attached to the bottom by pressing it against an o-ring. A carbon rod was used as the counter electrode (CE), and a saturated Ag/AgCl (3 M KCl) electrode was used as the reference electrode (RE); $E_{SHE} = 0.297$ V, set near the WE, to minimize the uncompensated IR drop. All potentials herein are referred to the Ag/AgCl (3 M KCl) scale. The area of the working electrode was 0.785 cm^2. All measurements were performed at ambient conditions.

One series of samples were allowed to rest at the open circuit potential (OCP) for 1 h to reach a quasi-steady state before performing potentiodynamic polarisation curve (PPC) measurements to assess the influence of the OCP stabilisation.

PPC measurements were conducted in the potential region starting from −150 mV vs. OCP to 1 V vs. reference electrode in the anodic direction until the current reached 1 mA or 1 V. The scan rate was 1 mV s^{-1}. Tafel extrapolation method to extract corrosion parameters (corrosion potential, E_{corr}, and corrosion current density, j_{corr}) from PPCs was performed using Nova 2.1 software, from which R_p and corrosion rates were calculated according to the standard ASTM G59–97 [50]. The repeatability of the measurements was satisfactory; representative results from repetitions are presented here. For corrosion rate calculations, equivalent weights (EW), defined as the molar mass divided by the number of transferred electrons, were those of the main alloy elements (Fe, Al and Zn).

Electrochemical measurements were conducted in solutions containing free F^- and Cl^-. Specifically, electrolytes were prepared using 0.0042 M and 0.0420 M solutions of hydrofluoric acid (HF) and hydrochloric acid (HCl), respectively. These solutions were further adjusted to a pH of 4 using approximately 0.0030 M and 0.0300 M of ammonium bicarbonate (NH_4HCO_3) for each acid. The rationale behind this electrolyte composition is outlined as follows:

Solutions were prepared to closely resemble those commonly used in studies on ZrCCs [25,51] but without H_2ZrF_6, thereby mimicking a "blank" fluoride solution to minimise the impact on the electrochemical double layer's composition. The decision not to study the combination of halide ions with the conversion H_2ZrF_6 agent was twofold and based on its non-activating and less aggressive nature. Firstly, the difference between the role of fluoride as an uncomplexed ion and as a component of hexafluorozirconate ion should be distinguished when considering the interaction with a metal surface. Whereas ZrF_6^{2-} contributes to enhanced hydrophilicity of the surface and interacts with the metal surface, resulting in the formation of a conversion coating, the role of free fluoride ions is mainly the thinning of the oxide layer formed on Al alloy [25,44]. Dissolution of Al-oxide in the presence of F^- results in the formation of soluble AlF_3 and AlF_6^{3-}, enhancing the role of attack [44]. It was shown that F^- at $\geq 10^{-6}$ M dramatically increases the dissolution rate of aluminium, which was ascribed to the high lability of monodentate surface complexes they form and their ability to penetrate the oxide layer structure, replacing oxygen atoms [52]. The second reason to perform the experiments without accounting for ZrF_6^{2-} was to avoid immediate surface passivation with ZrCCs at the OCP, making polarisation measurements unfeasible.

As noted at the beginning, free F^- ions, both pre-existing in formulations and released through the hydrolysis of H_2ZrF_6 from previous conversion processes, enable surface activation, and we concentrated on this effect. Consequently, we deliberately adjusted F^- concentrations in this study to mirror the highest 4 and lowest levels used in our preliminary studies (0.007 and 0.070 M). This adjustment was made under the assumption of complete H_2ZrF_6 hydrolysis, which typically does not occur [53,54], resulting in F^- levels six times higher than the selected H_2ZrF_6 concentrations of 0.007 and 0.070 M, giving 0.0042 and 0.0420 M, respectively [55,56].[1] These concentrations fall within the lower range observed in commercial ZrCC set-ups, as indicated by some of the available Safety Data Sheet (SDS) information. Typically, literature reports mention using concentrates containing H_2ZrF in the range of 10^{-2} to 10^{-1} M, with or without free F^- at levels around 10^{-2} M [57–62]. Since usually 1% of these concentrates are recommended for the preparation of commercial ZrCC baths, this translates to concentrations approximately ranging from 10^{-4} to 10^{-3} M for H_2ZrF_6 and 10^{-3} M for free F^-, respectively [57–62]. However, for improved corrosion protection properties, it would be advisable that further studies and commercial settings [61,62] also consider higher concentrations of H_2ZrF_6, Thus, this may lead to the adjustment of higher free F^- (10^{-2} M) concentration ranges that match those employed in the current study. Nonetheless, it was shown that higher concentrations (10^{-1}–10^{-2} M) of free F^- are detrimental to the film formation of ZrCC [27]. However, this observation was explicitly made on magnesium alloy and at significantly lower pH levels [27] and would require a further separate study on other materials.

A pH level of 4 was chosen [26], an intermediary value that conclusively promotes ZrCC deposition. This intermediary pH is expected to favour the deposition of ZrCC on various substrates andensure the complete dissociation of HF into free fluoride ions (pK_a value of HF = 3.18 [63]). For comparison, identical concentrations of Cl^- were employed alongside the same buffering agent and pH.

Finally, NH_4HCO_3 was used as the pH-adjusting agent, consistent with its common use in both commercial and homemade zirconium conversion baths [24], resulting in concentrations of 0.0030 M and 0.0300 M, which are presumably of a similar order of magnitude to those used in analogous H_2ZrF_6 solutions. Given its relatively high concentrations, comparable in magnitude to those of halide ions, the influence of NH_4HCO_3 on the equilibrium calculations was also considered. Consequently, separate calculations were conducted for the metal-H_2O, metal-F, metal-Cl, metal-NH_4HCO_3-F, and metal--NH_4HCO_3-Cl systems, depicted in the form of *E*-pH diagrams.

2.5. Equilibria diagrams

The chemical equilibrium diagrams in this study in the form of *E*-pH, predominance diagrams were created using Spana, a HALTAFALL-based [64] software. Spana is a Java version of the previous Medusa/Hydra tool [65,66], available under the GPLv3 license for free download at https://sites.google.com/site/chemdiagr/download. Although designed primarily for educational purposes, Spana offers a highly customisable database and an intuitive interface for generating equilibrium diagrams. All equilibrium constants in Spana are set at zero ionic strength, allowing for calculations across various pH levels and ionic strengths using either Davies equation, Specific Ion interaction Theory (SIT) or simplified Helgeson−Kirkham−Flowers (HKF) model, all based on Debye−Hückel theory [65,66]. Diagrams herein were produced using Spana's default database without altering or omitting any species with equilibrium constants mostly derived from B. Beverskog and I. Puigdomenech [67,68], the Organisation for Economic Co−operation and Development− Nuclear Energy Agency (OECD−NEA) [69,70], National

[1] General findings from X-ray photoelectron spectroscopy on the composition of ZrCCs, indicate a mixture predominantly composed of ZrO_2, along with smaller quantities of ZrF_4, oxyhydroxide, and/or oxyfluoride as a result of incomplete H_2ZrF_6 hydrolysis.

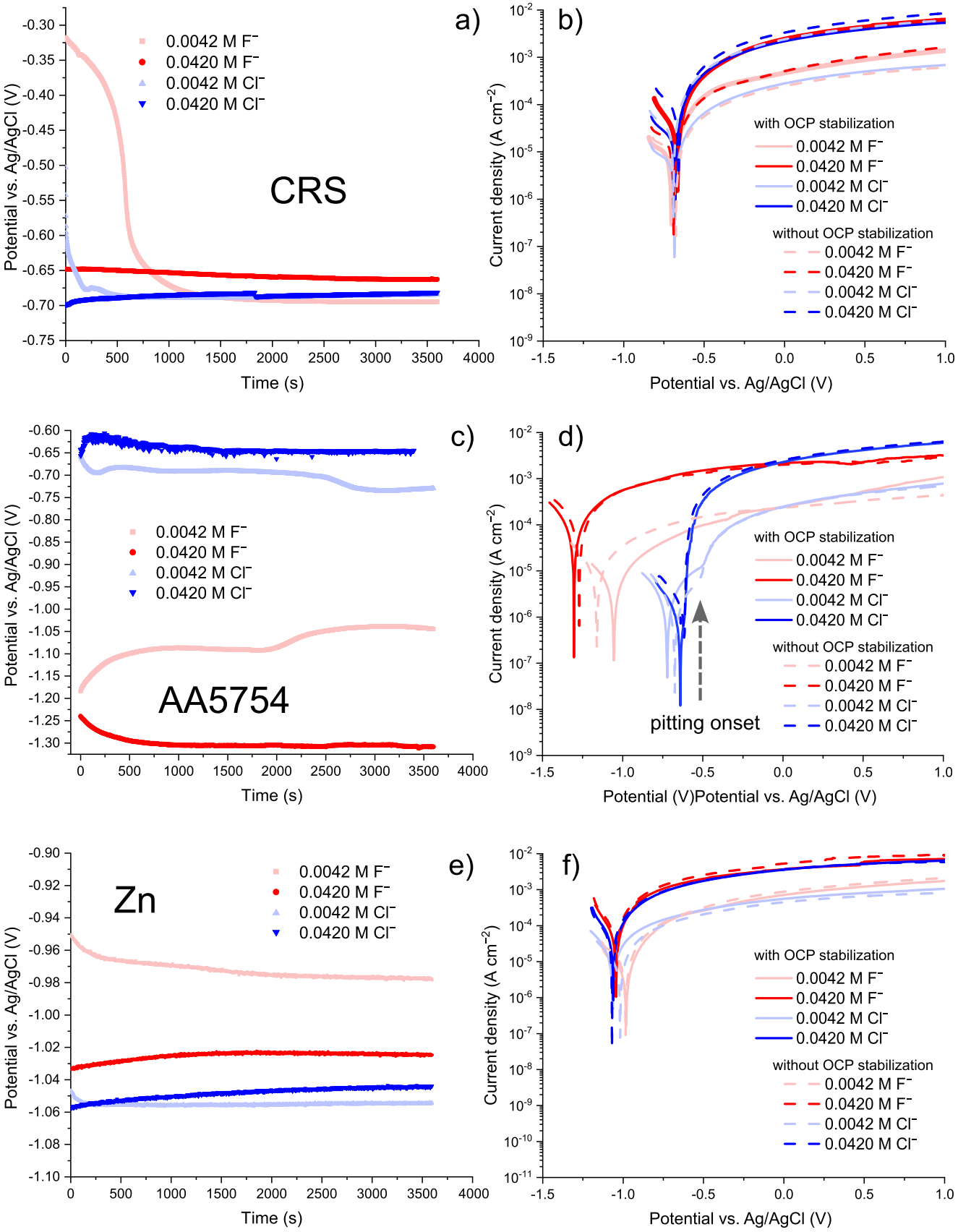

Fig. 1. Open circuit potential measurements (left) and potentiodynamic polarisation curves (right) of CRS, AA5754, and Zn in various solutions of F^- and Cl^-, with NH_4HCO_3 buffer at pH = 4. Please note that in (b), the solid red curves overlap with either the solid blue curve and the dashed red curve; they have been thickened for better visibility.

Institute of Standards and Technology (NIST) standard Reference Database [71], Brown and Ekberg [72], Baes and Mesmer [73] and Nordstrom and May [74] as well as other newer geochemical sources, including [75,76].

While Davies equation represents the simplest between them and is convenient for concentrations $\leq$ 0.1 molal, the HKF model generally performs well at low ionic strengths, as demonstrated with electrolytes at $\leq$ 0.2 molal [65] and a wide range of temperatures, making it suitable for this study's conditions in addition to its ease−of−use. On the other hand, SIT is a default model recommended in the Thermochemical Database (TDB) project of OECD–NEA [77,78] that uses specific ion−interaction parameters (ε) chosen to fit experimental data 25 °C. Notably, this model was found important and is described in more detail in our previous study on the aqueous chemistry of Zr [26]. Moreover, its application in this context led to the incorporation of a larger number of complexes, which, in our opinion, more accurately describe the observed behaviour, thereby justifying its use in this study as well (*vide infra*).

In particular, SIT accommodates both Debye−Hückel's long-range electrostatic interactions in dilute solutions and short-range non-electrostatic interactions at higher concentrations by employing ε, typically considered constant regardless of ionic strength. This makes SIT ideal for high-ionic-strength solutions and complex equilibria. More information on SIT, alongside other ionic strength correction models and reaction modelling in aqueous systems, can be found in [65,78]. Furthermore, Spana's default ionic strength calculations maintain electroneutrality by iteratively adding sodium or chloride ions as necessary, with ε derived from Hummel's [79] estimation method: $\varepsilon(Na^+, M^Y) = 0.05$ Y and $\varepsilon(M^Z, Cl^-) = -0.05 + (0.1\ Z)$, where Z and Y are the cation ($Z > 0$) and anion ($Y < 0$) electric charges, respectively. These default settings were maintained due to the ongoing uncertainty in updated SIT coefficients, especially concerning Fe-halide complexes, as indicated recently by NEA−OECD [69]. However, it is worth noting that despite convergence issues at extreme electrode potentials—i.e., outside the stability region of water [66] — the SIT model, by considering ionic strength effects, led to the occurrence of certain complexes (e.g. fluoride ones with Fe at lower potentials) in Pourbaix diagrams, similar to the findings of Xue et al. [7] albeit without formation of solid fluorides.

The total concentrations of dissolved substrate ions, namely Fe, Al, and Zn, used for constructing *E*-pH diagrams, were determined from an EQCM (Electrochemical Quartz Crystal Microbalance) study [35] of both commercial and homemade ZrCC baths, where a rough recalculation for the magnitude order for Fe dissolution gives the concentration of 10^{-6} M. This was particularly noted after 5 min conversion time, with mass losses increasing but staying within the same magnitude for longer times (more precisely, 9.13×10^{-7} M after 5 min, closer to industrially used conversion time, and 4.20×10^{-6} M after 30 min, respectively). Al and Zn were assumed to follow the same magnitude due to minor differences in mass losses compared to Fe. It should be noted that this study [35] only mentioned the use of Henkel's TecTalis® process [80] containing Cu without explicitly stating if the solutions used contained pre-added free fluoride. However, based on this limited data, we can infer the expected magnitude to perform equilibrium calculations that can further support our electrochemical findings. Nevertheless, this very concentration is also the standard threshold for corrosion defined by Pourbaix [81] and was used as the only concentration level for metal ions herein.

3. Results and discussion

3.1. Electrochemical results

Fig. 1a,c,f present OCP curves as a function of immersion time for CRS, AA5754 and Zn in Cl^- and F^- solutions of two concentrations. The OCP stabilisation occurs more rapidly at higher concentrations (0.0420 M) of both ions. In the case of the CRS substrate (Fig. 1a), all OCP values at the end of the 1 h-stabilization period show a minimal variation, with differences around 30 mV. The influence of F^- on the AA5754 substrate (Fig. 1c) reflects a noticeable reduction in OCP in the presence of F^-, with the most pronounced difference between concentrated F^- and Cl^- solutions being 665 mV and 314 mV for less concentrated solutions, both suggestive of a pronounced activation effect. For Zn substrates (Fig. 1e), Cl^- ions lead to a more negative OCP, with the largest difference being about 80 mV when compared to a 0.0042 M F^- and a 50 mV difference observed within F^- solutions, neither of which suggests a notable activation effect [82].

Fig. 1b,d,f shows that none of the substrates achieves proper passivation, as indicated by the high limiting current density values levelling off at more positive potentials, suggesting the formation of less protective surface films or adsorbed species. This is undoubtedly underscored by the formation of films directly from halide ion solutions without the pre-passivation in a halide-free medium, which would benefit the protective film development [14,83]. The respective OCP and PPCs data, along with their below-described results from Tafel extrapolation, are further illustrated in Fig. 2. Complete Tafel extrapolation results, with corrosion current densities recalculated to corrosion rates for inter-substrate comparison, are provided in Table 1.

A concentration of 0.0420 M of both Cl^- and F^- increases corrosion rates and decreases polarisation resistance across all substrates, while stabilisation at OCP generally mitigates corrosion rates (Fig. 1, Table 1).

In particular, from Figs. 1, 2 to Table 1, it is observed that CRS (Fig. 1b, Fig. 2) exhibits marginally higher corrosion rates with F^-than with Cl^-, especially at 0.0420 M, although E_{corr} remains stable at approximately −0.70 V. The absence of OCP 1 h-stabilization, however, leads to an increase in corrosion rates of 0.0420 M F^-solutions. For AA5754 (Figs. 1d, 2), F^-pronouncedly increases corrosion rates more than Cl^-, reflected also in more negative E_{corr} (up to −1.31 V for F^- versus around −0.65 V for Cl^-), indicating a less noble surface conducive to its activation role in the ZrCC process. Moreover, both ions at 0.0420 M increase Zn corrosion rates (Figs. 1f, 2), with F^-reaching rates of AA5754 and Cl^- exceeding those rates on both CRS and AA5754. However, the E_{corr} of Zn remains relatively unaffected, ranging between −0.982 and −1.085 V, though the highest Zn corrosion rates occur with 0.0420 M F^-without OCP stabilisation.

However, although OCP stabilisation does not lead to significant altering of corrosion rates, there is a subtle difference in the onset of limiting current (mass-transport controlled), specifically in the magnitude of limiting currents on CRS (Fig. 1b). Solutions containing Cl^- typically initiate limiting region at higher current densities, except in 0.0042 M, non-OCP-stabilised case. Conversely, F^- solutions generally induce limiting region onset at lower current densities. Only in the case

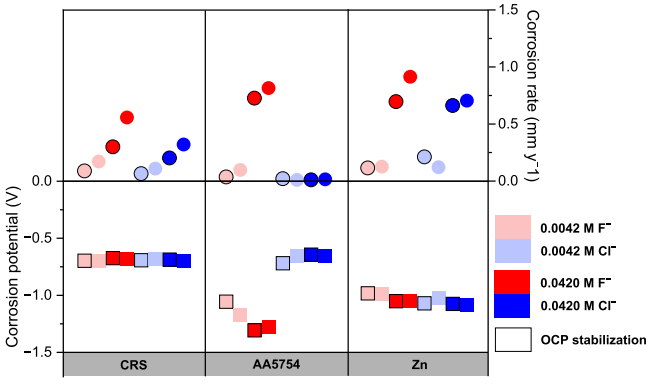

Fig. 2. Presentation of corrosion potential and corrosion rate for CRS, AA5754 and Zn substrates in F^- and Cl^- solutions of two concentrations (0.0420 and 0.0420 M) with and without 1 h-stabilisation at OCP. All electrochemical data are presented in Table 1.

Table 1
OCP and Tafel extrapolation results of PPCs for CRS, AA5754, and Zn in various solutions of F^- and Cl^-, with NH_4HCO_3 buffer at pH=4.

Substrate	Halide ion	Concentration (M)	OCP stabilization	E_{corr} (V)	i_{corr} (A)	j_{corr} (A/cm^2)	$\lvert b_a\rvert$ (V/dec)	$\lvert b_c\rvert$ (V/dec)	Polarisation resistance (Ωcm^2)	Corrosion rate (mm/year)
CRS	F^-	0.0042	no	−0.695	1.16E-05	1.48E-05	0.170	0.410	4491	0.172
	F^-	0.0420	no	−0.677	3.77E-05	4.80E-05	0.126	0.298	1019	0.558
	F^-	0.0042	yes	−0.697	6.07E-06	7.73E-06	0.102	0.466	6007	0.090
	F^-	0.0420	yes	−0.674	2.03E-05	2.59E-05	0.107	0.203	1496	0.301
	Cl^-	0.0042	no	−0.679	7.45E-06	9.49E-06	0.219	0.471	8706	0.110
	Cl^-	0.0420	no	−0.696	2.17E-05	2.76E-05	0.104	0.388	1647	0.321
	Cl^-	0.0042	yes	−0.693	4.45E-06	5.67E-06	0.138	0.444	10,286	0.066
	Cl^-	0.0420	yes	−0.687	1.37E-05	1.75E-05	0.080	0.326	2033	0.203
AA5754	F^-	0.0042	no	−1.168	7.01E-06	8.93E-06	0.281	0.227	7780	0.099
	F^-	0.0420	no	−1.276	5.79E-05	7.38E-05	0.244	0.197	818	0.816
	F^-	0.0042	yes	−1.056	2.67E-06	3.40E-06	0.188	0.208	16,094	0.038
	F^-	0.0420	yes	−1.306	5.17E-05	6.59E-05	0.256	0.214	979	0.728
	Cl^-	0.0042	no	−0.651	7.69E-07	9.79E-07	0.166	0.158	45,699	0.011
	Cl^-	0.0420	no	−0.652	1.17E-06	1.50E-06	0.041	0.175	12,249	0.017
	Cl^-	0.0042	yes	−0.718	1.54E-06	1.96E-06	0.204	0.231	30,503	0.022
	Cl^-	0.0420	yes	−0.643	8.44E-07	1.08E-06	0.043	0.204	18,197	0.012
Zn	F^-	0.0042	no	−0.986	6.67E-06	8.49E-06	0.160	0.226	6092	0.128
	F^-	0.0420	no	−1.045	5.22E-05	5.91E-05	0.113	0.150	602	0.889
	F^-	0.0042	yes	−0.982	4.64E-05	7.73E-06	0.181	0.439	9183	0.116
	F^-	0.0420	yes	−1.051	3.64E-05	4.64E-05	0.141	0.136	825	0.698
	Cl^-	0.0042	no	−1.024	6.36E-06	8.10E-06	0.174	0.211	6512	0.122
	Cl^-	0.0420	no	−1.086	3.69E-05	4.70E-05	0.178	0.167	1014	0.706
	Cl^-	0.0042	yes	−1.070	1.11E-05	1.42E-05	0.220	0.178	3848	0.213
	Cl^-	0.0420	yes	−1.075	3.48E-05	4.43E-05	0.173	0.154	1020	0.664

of 0.0420 M, OCP-stabilized F^- solution, the onset of the limiting region occurs at the same magnitude as that observed with Cl^- solutions.

For AA5754 (Figs. 1d, 2), F^- at 0.0420 M results in significantly higher corrosion current densities compared to equivalent concentrations of Cl^-, although lower F^- concentrations (0.0042 M) lead to similar current densities to Cl^- solutions. However, Cl^- solutions at 0.0420 M lead to pitting at around −0.5 V, whereas F^- solutions exhibit extended limiting current density regions despite higher corrosion current densities.

Lastly, in the case of Zn (Figs. 1f, 2), there is a notable impact of 0.0420 M of both ions on higher corrosion current densities regardless of OCP stabilisation, suggesting a general impact of ion concentration on corrosion rates.

It can be summarised that higher ion concentrations (0.0420 M) increase corrosion rates across all substrates. Ion type has no significant impact on CRS and Zn substrates but significantly influences the AA5754 substrate, where both ion type and concentration notably affect corrosion rates. However, further attention is needed to understand the effect of OCP stabilisation (*vide infra*).

3.2. Equilibrium calculations results

The enclosed *E*-pH diagrams for metal-H_2O systems (Fig. 3)[2] correspond fairly well with the existing ones [67,68,81]. In addition, using the SIT model agrees fairly well with applying HKF models for Fe and Zn [67,68].

3.2.1. *E*-pH diagrams for metal−H_2O

E-pH diagram for Fe is taken as a representative of CRS. Fig. 3a shows iron dissolves in acidic environments, forming Fe^{2+} and evolving hydrogen gas. At higher potentials in such conditions, Fe^{2+} oxidises to Fe^{3+} and $FeOH_2^+$, with Fe^{3+} only present at pH levels above zero. In alkaline solutions, iron achieves passivity, forming anionic complexes like $Fe(OH)_4^{2-}$ and $Fe(OH)_4^-$. In the passive region, ferrous hydroxide ($Fe(OH)_2$ (cr)) can oxidise to magnetite (Fe_3O_4 (cr)) at higher potentials, which can further oxidise to haematite (Fe_2O_3 (cr)), the most stable form at 25 °C. Finally, haematite dissolves at extremely high potentials to $Fe(OH)_4^{2-}$ [67].

E-pH diagram for Al is taken as a representation of AA5754. Fig. 3b shows aluminium dissolved as trivalent Al^{3+} ions in very acidic solutions and aluminate $Al(OH)_4^-$ ions in alkaline conditions.[3] Between pH 4 and 9, it forms an oxide film, typically of complex nature [81].

Fig. 3c shows that zinc does not passivate at a concentration of 10^{-6} M due to incorporating the uncharged aqueous hydrolysis complex $Zn(OH)_2$ in the *E*-pH diagrams. However, it is worth noting that zinc undergoes passivation at concentrations of $10^{-5.7}$ M, i.e. 2.51×10^{-6} M or higher, forming the oxide form, ZnO, that stabilises within a pH range of 8.2 − 12.1 at room temperature [68]. Since it is not impossible to achieve these concentrations in ZrCC conversion baths, further studies employing dissolution data on different substrates in ZrCCs are needed. It has been demonstrated that within the pH range 1–4, zinc corrosion is primarily controlled by cathodic mechanisms, with the hydrogen

[2] There is a significant difference in solubility between crystalline oxides and amorphous hydroxides. Amorphous hydroxides typically form initially at room temperature from fresh hydroxides, then slowly recrystallize into more insoluble and stable crystal solids [66]. Also, please do not confuse neutral species with solid ones, as the latter's state is clearly indicated by respective labels.

[3] To minimize calculation errors outside the water stability window [65], the potential range depicted in the Pourbaix diagrams does not encompass the potentials observed on AA5754 in this study, with the most negative being approximately −1.3 V vs. Ag/AgCl (3 M KCl), as indicated in Table 1, equivalent to about −1.5 V vs. SHE. However, the immunity region for aluminum, as would be obtained from the original Pourbaix diagram [81] below −1.6 V vs. SHE, makes further discussion of this region unnecessary.

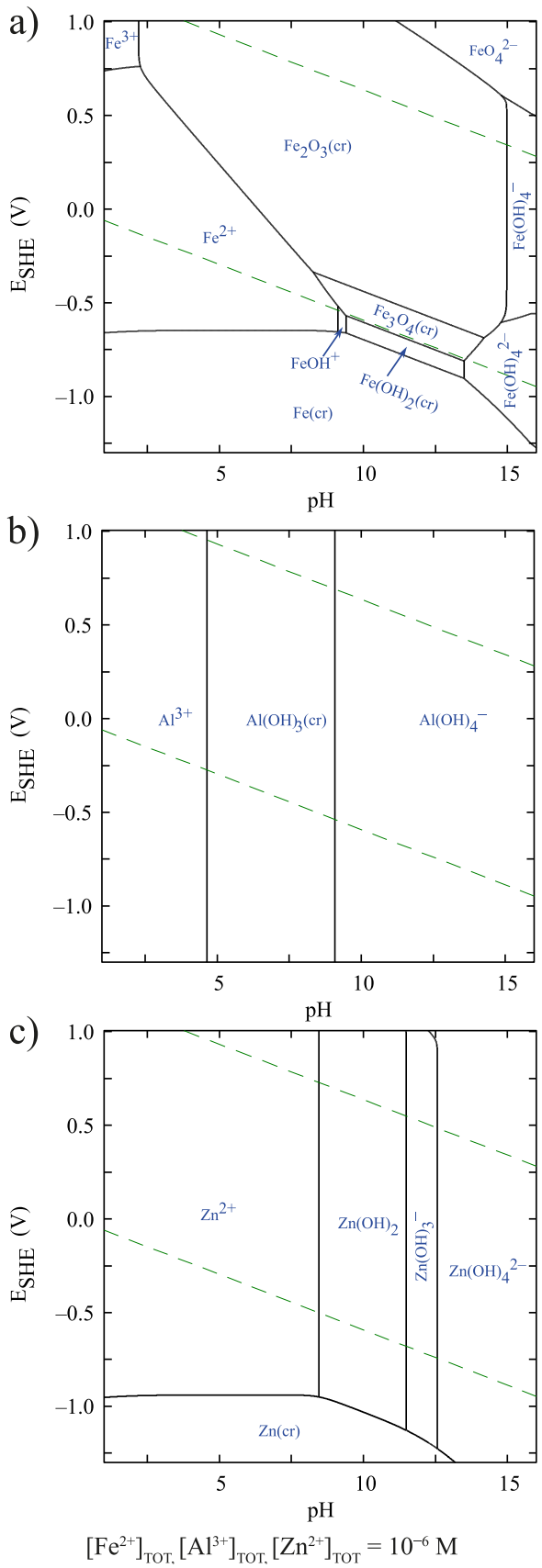

Fig. 3. Constructed *E*-pH diagrams for Fe (a), Al (b) and Zn (c) in H_2O at 10^{-6} M.

evolution reaction (HER) kinetics dictating the overall corrosion rates [84]. From pH 4 to 11, zinc's corrosion rates stabilize, attributed to the transition in the cathodic reaction from HER to the oxygen reduction reaction (ORR). However, the oxides formed in this range do not provide adequate corrosion protection [84]. In particular, at pH 12, the formation of an inner ZnO layer and an outer $Zn(OH)_2$ precipitated layer both contribute to a stable structure that acts as an effective anodic barrier. Conversely, at pH 13, the formation of soluble $Zn(OH)_3^-$ and $Zn(OH)_4^{2-}$ phases destabilizes the precipitated layer, leading to accelerated zinc corrosion. This layer further facilitates the catalysis of oxide growth through cathodic reactions [85].

3.2.2. *E-pH diagrams for metal-F, metal-Cl, metal-NH_4HCO_3-F, and metal-NH_4HCO_3-Cl systems*

From further comparison of *E*-pH (Pourbaix) diagrams within different systems (Figs. 3–6), it becomes apparent that while there is no discernible disparity in the visual representation between -H_2O and -Cl systems (Fig. 5), a notable contrast emerges within -F systems, particularly concerning CRS and AA5754 (Fig. 4a,b) in terms of F-complexation. Applying the Hard and Soft Acids and Bases principle (HSAB) [86], similar to our previous work on Zr [26], F-complexation leads to stable complexes, thereby extending the onset of hydrolysis and precipitation. In terms of corrosion, stable complexes may passivate the metal surface and inhibit further corrosion, while less stable complexes may dissolve and provide limited protection.

For Fe, a predominant F-complexation is observable, displacing the active region at higher potentials, which is in the absence of F^- occupied by Fe^{3+} (Fig. 4a). This phenomenon is further evident within the active corrosion region of Fe^{2+}, particularly pronounced in 0.0420 M F^- solution (Fig. 4b) ,[4] leading to the formation of FeF_3 complexes, which also aligns with E_{corr} region measured herein.

In the case of Al (Fig. 4c,d), as anticipated, the active corrosion region of Al^{3+} ions is significantly extended due to the presence of a series of F-complexes (AlF_2^+, AlF_3, AlF_4^-). This extension notably shrinks the passive region, with complexation intensifying at 0.0420 M and higher potentials (Fig. 4d), ultimately obscuring the original passive region altogether. This aligns with Chidambaram et al.'s findings [25], who observed that no passive Al film develops in solutions containing 0.024 M free F^-. This effect has otherwise significant applications in electrowinning in Zn electrolytes, where F^-facilitates Zn deposition on Al surfaces by removing the oxide layer from pure Al through F-complexation, as demonstrated in several instances, such as Xue et al. [7], Paula et al. [87] and Shen et al. [88].

Conversely, the integration of NH_4HCO_3 to equilibrium calculations of -F and -Cl systems, as depicted in Figs. 6 and 7, demonstrate minimal impact on CRS and AA5754, with the former exhibiting negligible formation of iron carbonate complexes, discernible as a narrow region between Fe^{2+} and Fe_2O_3 (cr). However, a substantial difference arises with Zn, where a series of carbonate and ammonium complexes are formed (Figs. 6e,f and 7e,f). The complexation with ammonium ions is

[4] Vertical dashed line between Fe^{2+} and FeF^+ mark the FeF^+ region disrupted by SIT convergence issues, likely due to model complexity. In addition, for Fe, there is scarce available data for aqueous fluoride complexes [69], which is further complicated by the fact that virtually no data are available below an ionic strength of 0.5 mol dm^{-3}. This makes extrapolation to zero ionic strength difficult due to the established dependence of ion interaction coefficients of halide anions and Fe^{3+} on ionic strength which is particularly pronounced for ionic strengths $\leq$ 0.5 [70], thus posing a question of the feasibility of the SIT model in this case. However, only the use of the SIT model resulted in the incorporation of F species in the OCP region, supporting electrochemical findings. Hence, while the HKF model balances accuracy with computational efficiency, the SIT model is preferred for systems exhibiting notable specific ion interactions, such as concentrated electrolytes or those with complex ions – precisely the case here – providing a more detailed description of solution behaviour (*vide supra*).

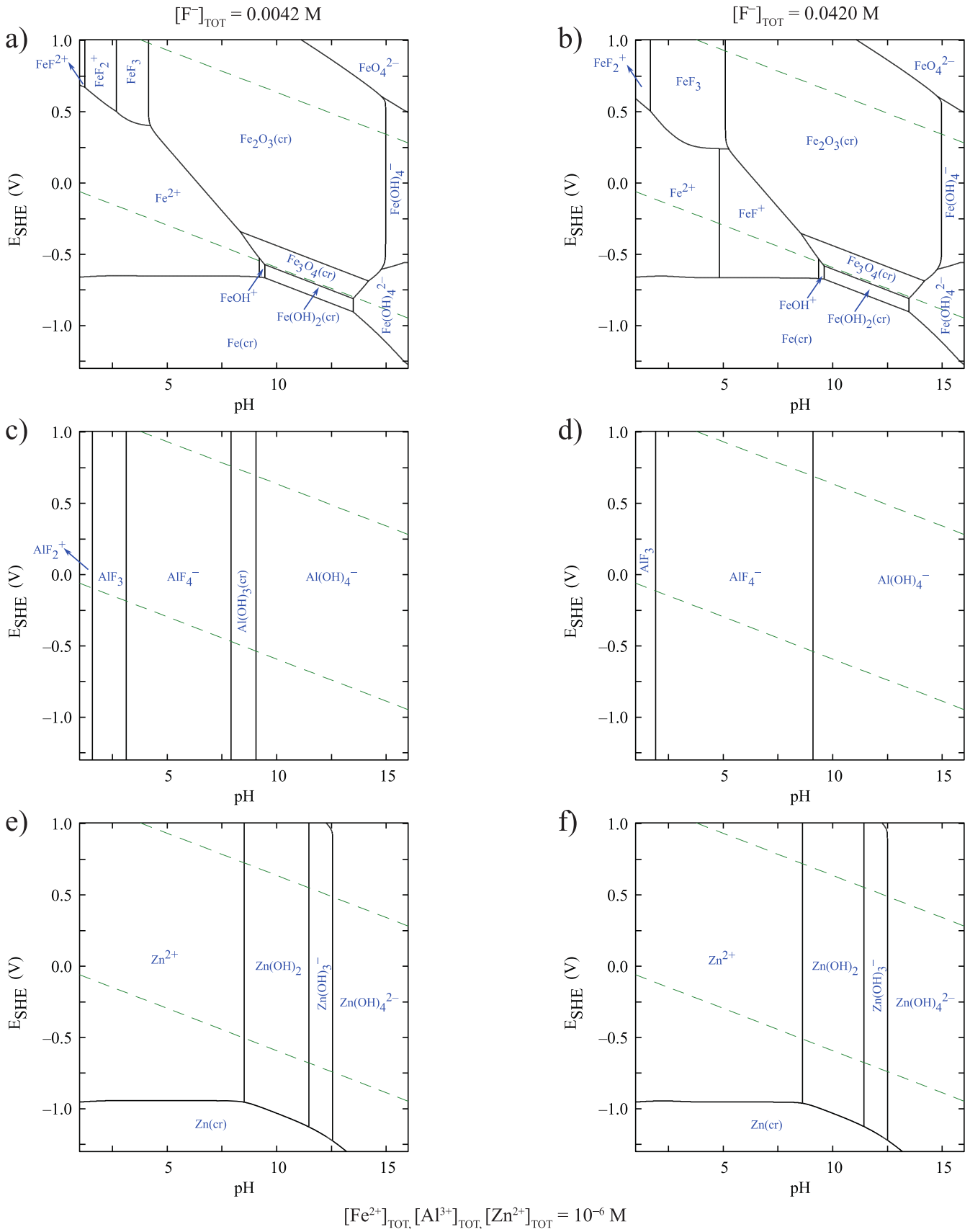

Fig. 4. Constructed *E*-pH diagrams for Fe (a,b), Al (c,d) and Zn (e,f) in the presence of F^- at 0.0042 M (left) and 0.0420 M (right).

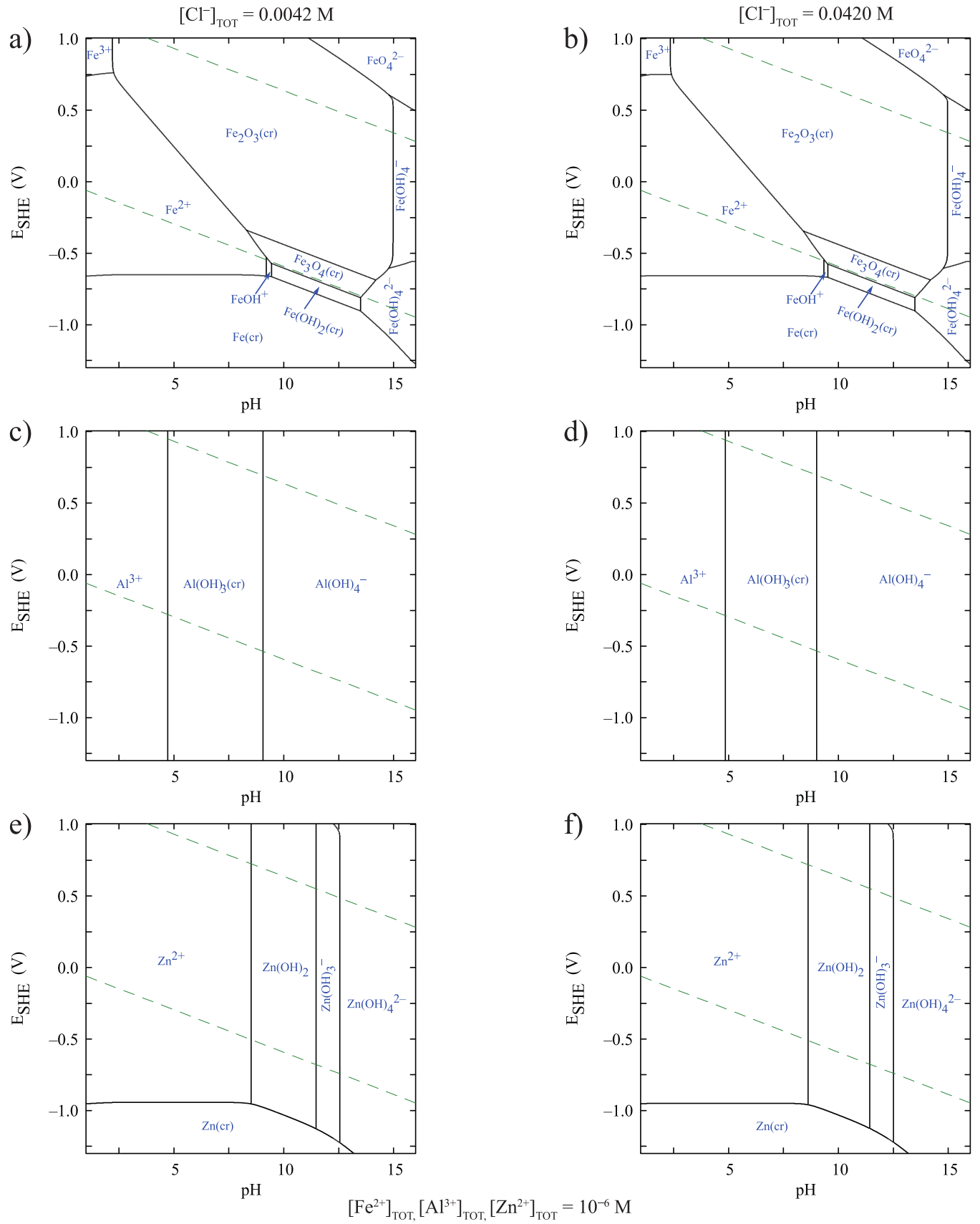

Fig. 5. Constructed *E*-pH diagrams for Fe (a,b), Al (c,d) and Zn (e,f) in the presence of Cl^- at 0.0042 M (left) and 0.0420 M (right).

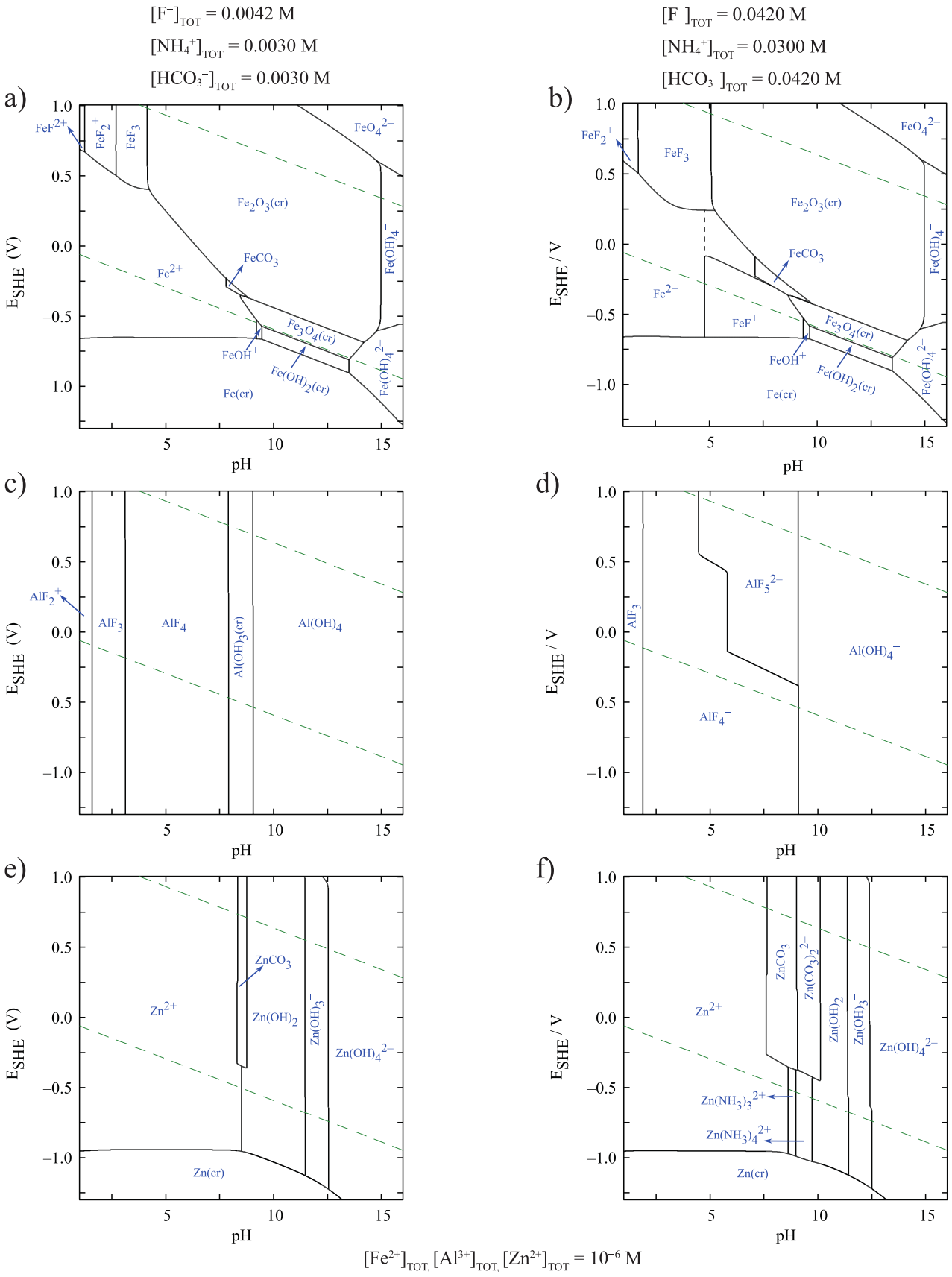

Fig. 6. Constructed *E*-pH diagrams for Fe (a,b), Al (c,d) and Zn (e,f) in the presence of $F^-$and NH_4HCO_3 at 0.0042 M (left) and 0.0420 M (right).

especially pronounced at a bicarbonate concentration of 0.0420 M, with regions that, under increased Zn concentrations, would be replaced by solid Zn carbonate and oxide species (not shown).

The graphs obtained contradict those of Xue et al. [3], wherein solid FeF_2 and ZnF_2 species are observed at F^- concentrations as low as 0.01 M In our view, this inconsistency stems from several factors. Firstly, older studies, including Xue et al.'s, relied on available equilibrium constants. Secondly, their calculations were conducted without ionic strength corrections, using equilibrium constants measured at varying ionic strengths. Additionally, Xue et al.'s approach of focusing on solids rather than metal ion concentrations,[5] coupled with limited consideration of aqueous species such as various hydrolysis products for iron and neutral aqueous complexes for zinc, as well as the omission of ions like sulphate ions.

3.3. Comparison of electrochemical and equilibrium data

The integration of electrochemical and thermodynamic data indicates that the effects of complexation on corrosion rates vary with the concentration of complexing ions and substrate type. Specifically, the formation of stable F-complexes on CRS at 0.0420 M may result in the lowest corrosion rates (Fig. 2) compared to the other two substrates studied. This is achieved by decreased free dissolved Fe due to complexation before reaching conditions for further predominant passivation by Fe_2O_3, as the diagrams in Figs. 4b and 6b predict. The diminishment of free Fe ions available for passivation could occur either when higher potentials (above ≈ 0.3 V vs. SHE) are reached or at the OCP/E_{corr} if an increase in pH (above ≈ 5) occurs during the anodic scan. Contrary to expectations, this F^- concentration does not result in lower limiting currents but rather corresponds to those observed in Cl^- solutions. In Cl^-solutions, in turn, the typically higher limiting currents compared to F^- solutions can be attributed to the absence of predominant complexation of Fe with Cl^-, likely resulting in more Fe available for oxidation during the anodic scan, except for the 0.0042 M non-OCP stabilized solution (Fig. 5a,b). Therefore, the additional F-complexation step at 0.0420 M, beginning at OCP and further enhanced by stabilisation, might delay the formation of the oxide layer during the anodic scan, as would be potentially expected based on the diagrams in Fig. 1b. Conversely, in Cl^- solutions, the absence of OCP stabilization at 0.0042 M not only leads to a lower amount of dissolved Fe but also seems to be low enough not to prevent the formation of the oxide surface layer. Here, the cosmotropic/chaotropic nature of Cl^- and F^- observed at alkaline pH [14] is not feasible due to complexation and subsequent passivation, both beginning in acidic solutions.

Similarly, for AA5754, no predominant Cl-complexation is observed (Fig. 5c,d), supporting quite low corrosion rates obtained. However, F-complexation (Fig. 4c,d) is significant throughout the entire active corrosion region of Al and becomes more pronounced at 0.0420 M and higher potentials. The complexation, which starts already at lower pH levels than those examined here and continues throughout the observed OCP and E_{corr} regions for both concentrations, might explain the negligible impact of OCP stabilization on the corrosion rates (Fig. 2). The higher corrosion current densities observed with 0.0420 M F^- compared to 0.0042 M F^- can be thus ascribed to the continuous formation of soluble F-complexes without any predominant passive region. On the contrary, it is undoubtedly that Cl^- induces pitting at 0.0420 M (Fig. 1d). Since *E*-pH diagrams, as predominance equilibria diagrams, do not represent kinetic and local effects, the possibility of the formation of Cl-complexes due to local effects within the pit cannot be excluded. Modelling pit behaviour would employ higher metal concentration to replicate pit conditions by constructing additional equilibrium diagrams, like fractional or logarithmic ones, like Thomas et al. [84]. Based on the literature reviewed, the corrosiveness of F^- towards Al predominantly manifests as complexation, resulting in more uniform corrosion, while its cosmotropic nature mitigates the aggressiveness towards pitting. In contrast, the impact of Cl^- is not observed in corrosion rates but rather in localized pitting, which is attributed to its chaotropic nature [13]. A higher affinity of Cl^- towards pitting on Al has been elaborated by Nguyen and Foley [89] and more recently by Natishan and O'Grady [9] as initial adherence to the surface oxide layer through electrostatic interactions at pH < 9. It was shown that Cl^- ions not only adsorb on the surface but are also incorporated into the oxide film, moving within across a range of electrical potentials, both below and above the pitting potential. This movement destabilizes the protective oxide layer by altering the film's resistivity and semiconducting properties, thereby making Al more susceptible to pitting. This can also lead to other physical disruptions, such as oxide blistering.

Lastly, the comparable effects of Cl^- and F^- on the corrosion rates of Zn, regardless of OCP stabilization, further enhanced at 0.0420 M, can be rather attributed to the effect of NH_4HCO_3, resulting in extensive hydrolysis of Zn with carbonate and ammonium species at higher and lower potentials, respectively. The question remains whether the pH for this complexation is indeed reached during polarisation, given its higher values compared to Fe and Al. Hence, it can be articulated that zinc's corrosion rates increase with solution ionic strength. In terms of ZrCCs, however, this complexation would occur at a pH higher than that of zirconia precipitation, as shown in our previous work [26], thus not affecting the conversion process.

Predicting effects of Cl^- and F^- on ZrCC can be explained through incomplete hydrolysis of H_2ZrF_6 [54], as well as incomplete removal during rinsing through an exchange with hydroxide ions, leading to the existence of a certain amount of residual F^-in the form of zirconium oxyfluorides in ZrCCs [90]. However, F^-tends to exchange less rapidly than Cl^-, enabling the latter to eventually replace fluoride in the ZrCC films through the outer ligand sphere [91] over time, as confirmed by Šekularac et al. [92,93]. Interestingly, while X-ray photoelectron spectroscopy revealed the presence of ZrO_2, ZrF_4, and other compounds in Zr conversion coatings [55,56], analogous Ti conversion coatings employing H_2TiF_6 were found only to incorporate TiO_2 [55].

The only study currently available, conducted by Li, Desouza, and Swain, has shown that the deposition of Ti- and trivalent chromium-based conversion coatings, both also containing ZrF_6^{2-}, is governed by a local pH change. This change is induced by the increased formation of hydroxyl ions during the cathodic reaction of oxygen reduction, where the pH increased from 3.9 in the bulk bath to nearly 7 and 8.5, respectively [94]. Conversely, high polarization potentials were not observed during the ZrCC process. Instead, this process occurs at the OCP values [36], consistent with the OCP/E_{corr} values for each substrate obtained herein. Therefore, our future research endeavours will aim to determine how much the pH can increase during the ZrCC process in ZrF_6^{2-} solutions with an NH_4HCO_3 buffer. Such studies could then be supported by the thermodynamic analysis presented herein for Fe and Zn, whose complexation reactions are pH-dependant, in contrast to Al, which exhibits consistent complexation throughout the entire operating *E*-pH range.

Nevertheless, the main idea of this article relies on the concept that the effect of ZrF_6^{2-} ions is not evident in predominance diagram calculations and was instead investigated as the effect of the more aggressive free fluoride ions that are liberated from ZrF_6^{2-} hydrolysis and are also added by default in some commercial ZrCC formulations. Thus, we firmly believe this study can be used to predict ZrCC bath behaviour on different substrates further. In any case, it can certainly be used as a separate study of the sole effects of the halide ions of interest on the substrates discussed herein.

[5] Studying metal complex formation and solubility at low concentrations, like 10^{-6} M, offers a clearer insight into metal behaviour in solutions, avoiding the complications from surface phenomena and microstructural effects seen in solid species. Nonetheless, the letter is crucial for precipitation studies [66].

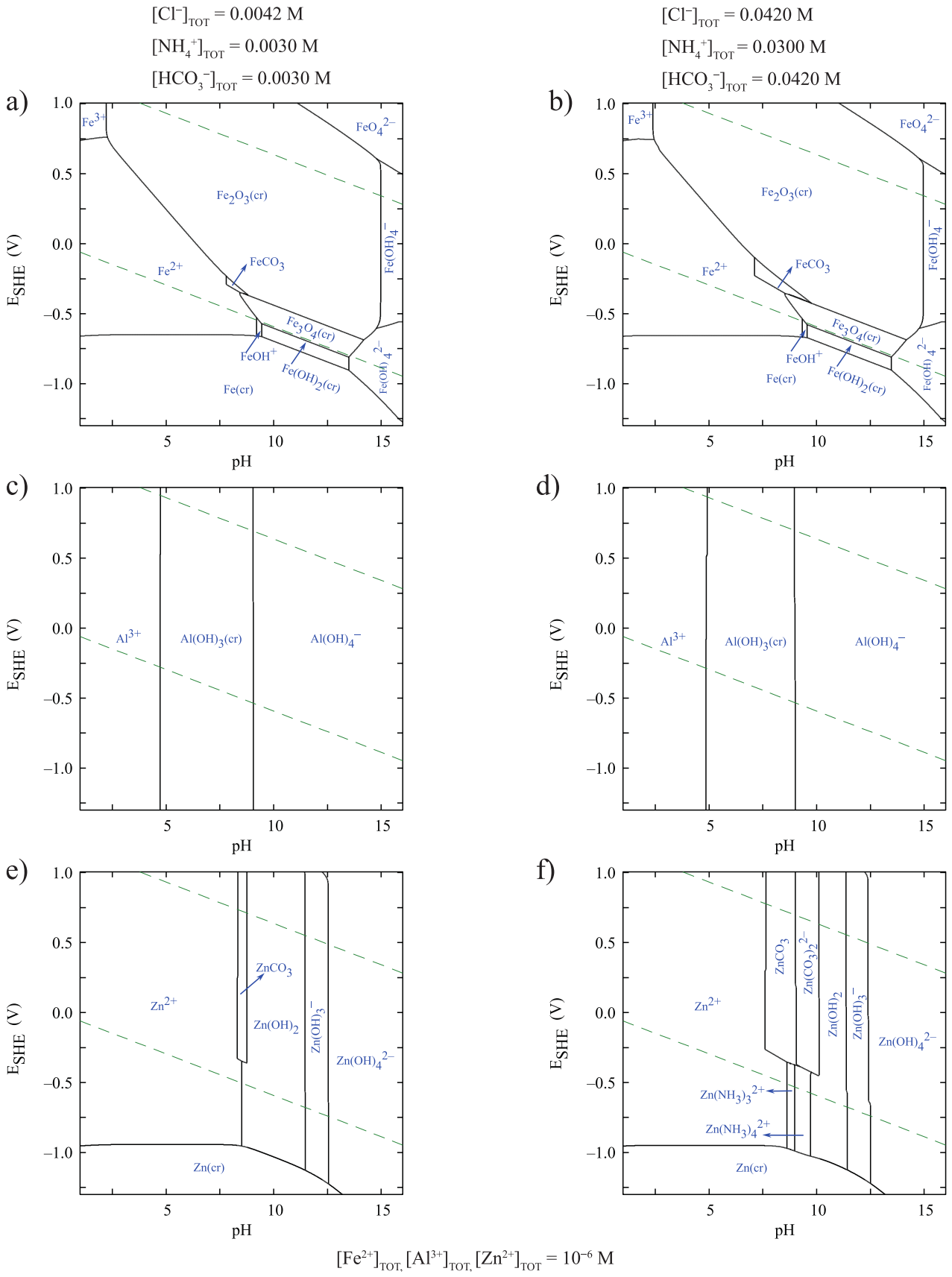

Fig. 7. Constructed *E*-pH diagrams for Fe (a,b), Al (c,d) and Zn (e,f) in the presence of $Cl^-$and NH_4HCO_3 at 0.0042 M (left) and 0.0420 M (right).

4. Conclusions

This study investigated the corrosion behaviour of three substrates—CRS, AA5754 and Zn—in environments containing F^- and Cl^- at 0.0042 and 0.0420 M concentrations in the presence of 0.0030 and 0.030 M ammonium bicarbonate at pH = 4, both with and without OCP stabilization. The generally observed electrochemical actions of F^- and Cl^- have been confirmed herein; however, they are further supported by thermodynamic calculations that considered the entire solution composition and ion interactions in much more complex equilibria.

For CRS, stable F-complex formation reduces corrosion rates by decreasing the amount of freely dissolved iron during anodic scans, thereby aiding the formation of the surface layer with insufficient protective properties. However, this process is less pronounced when complexation occurs in an OCP-stabilised 0.0420 M F^- solution. Conversely, Cl^- ions only reduce corrosion rates in 0.0042 M Cl^- non-OCP stabilized solution, indicating a balance between reduced free Fe availability and Cl^- concentration that does not interfere with the formation of the surface layer.

With AA5754, the effect of ion concentration is more pronounced. Due to complexation, 0.0420 M of F^- results in considerably greater corrosion rates than Cl^-. At 0.0042 M, however, the corrosive effects of F^- and $Cl^-$are similar. Notably, Cl^- at 0.0420 M leads to pitting corrosion, while F^-induces a more extended limiting current range, suggesting a more uniform corrosion process, conforming to their inherent differences in cosmotropic/chaotropic behaviour.

In the case of Zn, corrosion rates appear to be unaffected by the type of halide ion. Here, the advantage of thermodynamic calculations truly becomes apparent, as they indicate that the observed corrosion phenomenon can be due to the buffer, i.e., the formation of complexes with ammonium and carbonate ions, which further increases at 0.0420 M of NH_4HCO_3.

F-complexation, depicted in predominance diagrams and reflected in uniform corrosion of Fe and Al, occurs at pH levels achievable during polarization. However, for Zn, buffer-complexation occurs at a higher pH that might not be encountered during polarization, thereby making it safer to say its behaviour is influenced by higher ionic strength.

Nevertheless, despite the inability to account for pitting behaviour in thermodynamic diagrams, considering complex equilibria supports the stabilisation effects on OCP and the differences in corrosion rates. Most importantly, it also aids in explaining that zinc's corrosion behaviour is influenced by ammonium bicarbonate complexation rather than halide ions.

As such, this study emphasises the significance of accounting for complex equilibria in corrosion analysis, offering a framework for future studies, particularly those addressing intricate solutions with conversion agents and additives in coating baths.

CRediT authorship contribution statement

Ana Kraš: Writing – review & editing, Writing – original draft, Methodology, Formal analysis, Conceptualization. **Ingrid Milošev:** Writing – review & editing, Validation, Supervision, Methodology, Funding acquisition, Conceptualization.

Declaration of competing interest

The authors declare that they have no known competing financial interests or personal relationships that could have appeared to influence the work reported in this paper.

Data availability

Data will be made available on request.

Acknowledgements

This research was funded by the Slovenian Research and Innovation Agency through the research core funding grant P2–0393 and project PR-09806. The authors wish to thank Dr. Sviatlana V. Lamaka of the Helmholtz-Zentrum Hereon, Geesthacht, Germany, for providing insights on the influence of bicarbonate ions on Zn, which ultimately led to the extension of this study.

References

[1] H.H. Strehblow, B. Titze, B.P. Loechel, The breakdown of passivity of iron and nickel by fluoride, Corros. Sci. 19 (1979) 1047–1057, https://doi.org/10.1016/S0010-938X(79)80094-3.
[2] H.H. Strehblow, Mechanisms of pitting corrosion, P. Marcus (Ed.). Corrosion Mechanisms in Theory and Practice, 2nd ed., CRC Press, Boca Raton, 2002, p. 44.
[3] B. Löchel, H.H. Strehblow, Breakdown of passivity of iron by fluoride, Electrochim. Acta 28 (1983) 565–571, https://doi.org/10.1016/0013-4686(83)85043-9.
[4] K.E. Heusler, L. Fischer, Kinetics of pit initiation at passive iron, Mater. Corros. 27 (1976) 551–556, https://doi.org/10.1002/maco.19760270802.
[5] K.F. Lorking, J.E.O. Mayne, The corrosion of aluminium in solutions of sodium fluoride and sodium chloride, Br. Corros. J. 1 (1966) 181–182, https://doi.org/10.1179/000705966798327795.
[6] A.F. Beck, M.A. Heine, D.S. Keir, D. van Rooyen, M.J. Pryor, Further studies of the electrical characteristics of oxide films on aluminium, Corros. Sci. 2 (1962) 133–145, https://doi.org/10.1016/0010-938X(62)90005-7.
[7] T. Xue, W.C. Cooper, R. Pascual, S. Saimoto, Effect of fluoride ions on the corrosion of aluminium in sulphuric acid and zinc electrolyte, J. Appl. Electrochem. 21 (1991) 238–246, https://doi.org/10.1007/BF01052577.
[8] M.F. Abd Rabbo, J.A. Richardson, G.C. Wood, A study of conversion coating development on aluminium in chromate/fluoride solutions using secondary ion mass spectrometry, Corros. Sci. 18 (1978) 117–123, https://doi.org/10.1016/S0010-938X(78)80082-1.
[9] P.M. Natishan, W.E. O'Grady, Chloride ion interactions with oxide-covered aluminum leading to pitting corrosion: a review, J. Electrochem. Soc. 161 (2014) C421–C432, https://doi.org/10.1149/2.1011409jes.
[10] J.A. Richardson, G.C. Wood, The interpretation of impedance changes on oxide-coated aluminum produced by immersion in inhibitive and corrosive aqueous media, J. Electrochem. Soc. 120 (1973) 193–201, https://doi.org/10.1149/1.2403419.
[11] W.M. Carroll, M. Murphy, C.B. Breslin, The corrosion/dissolution behaviour of aluminium in solutions containing both chloride and fluoride ions, Corros. Sci. 34 (1993) 1495–1507, https://doi.org/10.1016/0010-938X(93)90244-B.
[12] P. Guo, E.C. La Plante, B. Wang, X. Chen, M. Balonis, M. Bauchy, G. Sant, Direct observation of pitting corrosion evolutions on carbon steel surfaces at the nano-to-micro- scales, Sci. Rep. 8 (2018) 7990, https://doi.org/10.1038/s41598-018-26340-5.
[13] J.L. Trompette, L. Arurault, S. Fontorbes, L. Massot, Influence of the anion specificity on the electrochemical corrosion of anodized aluminum substrates, Electrochim. Acta 55 (2010) 2901–2910, https://doi.org/10.1016/j.electacta.2009.12.063.
[14] J.L. Trompette, Implications of the kosmotrope/chaotrope nature of the anions on the breakdown of passivity of iron by halides, Corros. Sci. 82 (2014) 108–114, https://doi.org/10.1016/j.corsci.2014.01.005.
[15] S.Y. Yu, W.E. O'Grady, D.E. Ramaker, P.M. Natishan, Chloride ingress into aluminum prior to pitting corrosion An investigation by XANES and XPS, J. Electrochem. Soc. 147 (2000) 2952–2958, https://doi.org/10.1149/1.1393630.
[16] B. Zhang, Y. Li, F. Wang, Electrochemical behaviour of microcrystalline aluminium in neutral fluoride containing solutions, Corros. Sci. 51 (2009) 268–275, https://doi.org/10.1016/j.corsci.2008.11.016.
[17] R. Elaish, M. Curioni, K. Gowers, A. Kasuga, H. Habazaki, T. Hashimoto, P. Skeldon, Effects of fluoride ions in the growth of barrier-type films on aluminium, Electrochim. Acta 245 (2017) 854–862, https://doi.org/10.1016/j.electacta.2017.06.034.
[18] G.I. Ashok Kumar, A. Lambert, J. Caperton, M. Asokan, W. Yi, O. Chyan, Comparative study of chloride and fluoride induced aluminum pad corrosion in wire-bonded device packaging assembly, Corros. Mater. Degrad. 2 (2021) 447–460, https://doi.org/10.3390/cmd2030023.
[19] M. Pagitsas, General and pitting corrosion deduced from current oscillations in the passive–active transition state of the Fe|H_2SO_4 electrochemical system, Electrochim. Acta 47 (2002) 4163–4179, https://doi.org/10.1016/S0013-4686(02)00412-7.
[20] T.C. Chen, T.Y. Yung, C.C. Chou, Y.M. Wang, Investigating the corrosion resistance of Zn and Al coating deposited by arc thermal spraying process, Surf. Coat. Technol. 484 (2024) 130684, https://doi.org/10.1016/j.surfcoat.2024.130684.
[21] R. Ramanauskas, L. Muleshkova, L. Maldonado, P. Dobrovolskis, Characterization of the corrosion behaviour of Zn and Zn alloy electrodeposits: atmospheric and accelerated tests, Corros. Sci. 40 (1998) 401–410, https://doi.org/10.1016/S0010-938X(97)00144-3.
[22] P. De Lima-Neto, A.N. Correia, R.P. Colares, W.S. Araujo, Corrosion study of electrodeposited Zn and Zn-Co coatings in chloride medium, J. Braz. Chem. Soc. 18 (2007) 1164–1175, https://doi.org/10.1590/S0103-50532007000600010.

[23] M. Prestat, J. SoaresCosta, B. Lescop, S. Rioual, L. Holzer, D. Thierry, Cathodic corrosion of zinc under potentiostatic conditions in NaCl solutions, ChemElectroChem 5 (2018) 1203–1211, https://doi.org/10.1002/celc.201701325.
[24] I. Milošev, G.S. Frankel, Review—conversion coatings based on zirconium and/or titanium, J. Electrochem. Soc. 165 (2018) C127–C144, https://doi.org/10.1149/2.0371803jes.
[25] D. Chidambaram, C.R. Clayton, G.P. Halada, The role of hexafluorozirconate in the formation of chromate conversion coatings on aluminum alloys, Electrochim. Acta 51 (2006) 2862–2871, https://doi.org/10.1016/j.electacta.2005.08.022.
[26] A. Kraš, I. Milošev, The Aqueous chemistry of zirconium as a basis for better understanding the formation of zirconium conversion coatings: updated thermodynamic data, J. Electrochem. Soc. 170 (2023) 21508, https://doi.org/10.1149/1945-7111/acb9c2.
[27] S. Verdier, N. van der Laak, F. Dalard, J. Metson, S. Delalande, An electrochemical and SEM study of the mechanism of formation, morphology, and composition of titanium or zirconium fluoride-based coatings, Surf. Coat. Technol. 200 (2006) 2955–2964, https://doi.org/10.1016/j.surfcoat.2004.10.139.
[28] T. Rodney, Fluorinated acid compounds, compositions and methods of use, WO2018104796A1, 2017.
[29] H. Eivaz Mohammadloo, A.A. Sarabi, Ti-based conversion coatings on cold-rolled steel substrate: the effect of practical parameters and Ti source on surface and electrochemical properties, Corrosion 72 (2016) 791–804, https://doi.org/10.5006/1936.
[30] B. Szczygieł, J. Winiarski, W. Tylus, Effect of deposition time on morphology, corrosion resistance and mechanical properties of Ti-containing conversion coatings on zinc, Mater. Chem. Phys. 129 (2011) 1126–1131, https://doi.org/10.1016/j.matchemphys.2011.05.074.
[31] Y.T. Tsai, K.H. Hou, C.Y. Bai, J.L. Lee, M.D. Ger, The influence on immersion time of titanium conversion coatings on electrogalvanized steel, Thin Solid Films 518 (2010) 7541–7544, https://doi.org/10.1016/j.tsf.2010.05.042.
[32] L. Zhu, F. Yang, N. Ding, Corrosion resistance of the electro-galvanized steel treated in a titanium conversion solution, Surf. Coat. Technol. 201 (2007) 7829–7834, https://doi.org/10.1016/j.surfcoat.2007.03.024.
[33] H. Eivaz Mohammadloo, A.A. Sarabi, Titanium composite conversion coating formation on CRS In the presence of Mo and Ni ions: electrochemical and microstructure characterizations, Appl. Surf. Sci. 387 (2016) 252–259, https://doi.org/10.1016/j.apsusc.2016.06.095.
[34] J.E. Huheey, E.A. Keiter, R.L. Keiter, O.K. Medhi, Inorganic Chemistry: Principles of Structure and Reactivity, 4th ed., HarperCollins College Publishers, New York, 1993.
[35] S. Adhikari, K.A. Unocic, Y. Zhai, G.S. Frankel, J. Zimmerman, W. Fristad, Hexafluorozirconic acid based surface pretreatments: characterization and performance assessment, Electrochim. Acta 56 (2011) 1912–1924, https://doi.org/10.1016/j.electacta.2010.07.037.
[36] J. Cerezo, I. Vandendael, R. Posner, K. Lill, J.H.W. de Wit, J.M.C. Mol, H. Terryn, Initiation and growth of modified Zr-based conversion coatings on multi-metal surfaces, Surf. Coat. Technol. 236 (2013) 284–289, https://doi.org/10.1016/j.surfcoat.2013.09.059.
[37] O. Lunder, C. Simensen, Y. Yu, K. Nisancioglu, Formation and characterisation of Ti–Zr based conversion layers on AA6060 aluminium, Surf. Coat. Technol. 184 (2004) 278–290, https://doi.org/10.1016/j.surfcoat.2003.11.003.
[38] A. Sarfraz, R. Posner, M.M. Lange, K. Lill, A. Erbe, Role of intermetallics and copper in the deposition of ZrO_2 conversion coatings on AA6014, J. Electrochem. Soc. 161 (2014) C509–C516, https://doi.org/10.1149/2.0121412jes.
[39] J. Cerezo, P. Taheri, I. Vandendael, R. Posner, K. Lill, J.H.W. de Wit, J.M.C. Mol, H. Terryn, Influence of surface hydroxyls on the formation of Zr-based conversion coatings on AA6014 aluminum alloy, Surf. Coat. Technol. 254 (2014) 277–283, https://doi.org/10.1016/j.surfcoat.2014.06.030.
[40] H. Eivaz Mohammadloo, A.A. Sarabi, A.A. Sabbagh Alvani, H. Sameie, R. Salimi, Nano-ceramic hexafluorozirconic acid based conversion thin film: surface characterization and electrochemical study, Surf. Coat. Technol. 206 (2012) 4132–4139, https://doi.org/10.1016/j.surfcoat.2012.04.009.
[41] H. Eivaz Mohammadloo, A.A. Sarabi, R.Mohammad Hosseini, M. Sarayloo, H. Sameie, R. Salimi, A comprehensive study of the green hexafluorozirconic acid-based conversion coating, Prog. Org. Coat. 77 (2014) 322–330, https://doi.org/10.1016/j.porgcoat.2013.10.006.
[42] Y. Guan, J. Liu, C. Yan, Novel Ti/Zr based non-chromium chemical conversion coating for the corrosion protection of electrogalvanized steel, Int. J. Electrochem. Sci. 6 (2011) 4853–4867, https://doi.org/10.1016/S1452-3981(23)18372-6.
[43] H.R.P. Cardoso, C. Rapacki, J.Z. Ferreira, Monitoring of a Zr-based conversion coating on galvanised steel and its performance against corrosion, Corros. Eng. Sci. Technol. 54 (2019) 726–730, https://doi.org/10.1080/1478422X.2019.1657703.
[44] P. Campestrini, E.P.M. van Westing, J.H.W. de Wit, Influence of surface preparation on performance of chromate conversion coatings on Alclad 2024 aluminium alloy: part I: nucleation and growth, Electrochim. Acta 46 (2001) 2553–2571, https://doi.org/10.1016/S0013-4686(01)00475-3.
[45] SurTec International GmbH, Technical Data Sheet for SurTec® 132 Liquid Recyclable Builder, (2021).
[46] SurTec International GmbH, Technical Data Sheet for SurTec® 089 Recyclable Detergent Component, (2021).
[47] SurTec International GmbH, Technical Data Sheet for SurTec® 496 High End Desmutting, (2021).
[48] SurTec International GmbH, Technical Data Sheet for SurTec® 141 Alkaline Builder, (2021).
[49] G.S. Frankel, M. Rohwerder, Electrochemical techniques for corrosion, M. Stratmann, G. Frankel (Eds.). Encyclopedia of Electrochemistry, Wiley, Weinheim, 2003, https://doi.org/10.1002/9783527610426.bard040007.
[50] ASTM International, ASTM G59-97(2020), Standard Test Method for Conducting Potentiodynamic Polarization Resistance Measurements, (2023). 10.1520/G0059-97R20.
[51] D.F. Roeper, D. Chidambaram, C.R. Clayton, G.P. Halada, Development of an environmentally friendly protective coating for the depleted uranium–0.75wt.% titanium alloy, Electrochim. Acta 51 (2005) 545–552, https://doi.org/10.1016/j.electacta.2005.05.015.
[52] V. Žutić, W. Stumm, Effect of organic acids and fluoride on the dissolution kinetics of hydrous alumina. A model study using the rotating disc electrode, Geochim. Cosmochim. Acta 48 (1984) 1493–1503, https://doi.org/10.1016/0016-7037(84)90405-8.
[53] M.A. Fedotov, A.V. Belyaev, A study of the hydrolysis of ZrF_6^{2-} and the structure of intermediate hydrolysis products by ^{19}F and ^{91}Zr NMR in the 9.4 T field, J. Struct. Chem. 52 (2011) 69–74, https://doi.org/10.1134/S0022476611010094.
[54] V.P. Tolstoi, B. Altangerel, Hydrolysis of ZrF_6^{2-} anions in solutions of copper(II) ammine and synthesis of $Cu_xZr(OH)_yF_z$ nanolayers by the ionic layering method, Russ. J. Gen. Chem. 76 (2006) 1716–1718, https://doi.org/10.1134/S1070363206110065.
[55] S. Verdier, S. Delalande, N. van der Laak, J. Metson, F. Dalard, Monochromatized x-ray photoelectron spectroscopy of the AM60 magnesium alloy surface after treatments in fluoride-based Ti and Zr solutions, Surf. Interface Anal. 37 (2005) 509–516, https://doi.org/10.1002/sia.2042.
[56] M. Mujdrica Kim, B. Kapun, U. Tiringer, G. Šekularac, I. Milošev, Protection of aluminium alloy 3003 in sodium chloride and simulated acid rain solutions by commercial conversion coatings containing Zr and Cr, Coatings 9 (2019) 563, https://doi.org/10.3390/coatings9090563.
[57] Mavom Chemie B.V., Safety Data Sheet for MAVOMcoat 160, (2015).
[58] Mavom Chemie B.V., Safety Data Sheet for MAVOMcoat 1700, (2017).
[59] Henkel Corporation, Safety Data Sheet for BONDERITE M-NT 1, (2018).
[60] Henkel Corporation, Technical Data Sheet for BONDERITE M-NT 1, (2016).
[61] SurTec International GmbH, Safety Data Sheet for SurTec® 650 chromitAL TCP, (2021).
[62] SurTec International GmbH, Technical Data Sheet for SurTec® 650 chromitAL TCP, (2021).
[63] Ralph.H. Petrucci, W.S. Harwood, F.G. Herring, General Chemistry: Principles and Modern Applications, 8th ed., Prentice Hall, New Jersey, 2002.
[64] N. Ingri, W. Kakolowicz, L.G. Sillén, B. Warnqvist, High-speed computers as a supplement to graphical methods—V1Haltafall, a general program for calculating the composition of equilibrium mixtures, Talanta 14 (1967) 1261–1286, https://doi.org/10.1016/0039-9140(67)80203-0.
[65] I. Puigdomènech, E. Colàs, M. Grivé, I. Campos, D. García, A tool to draw chemical equilibrium diagrams using SIT: applications to geochemical systems and radionuclide solubility, MRS Online Proc. Libr. 1665 (2014) 111–116, https://doi.org/10.1557/opl.2014.635.
[66] I. Puigdomènech, Spana, (2020). https://sites.google.com/site/chemdiagr/home/java-versions.
[67] B. Beverskog, I. Puigdomenech, Revised pourbaix diagrams for iron at 25–300°C, Corros. Sci. 38 (1996) 2121–2135, https://doi.org/10.1016/S0010-938X(96)00067-4.
[68] B. Beverskog, I. Puigdomenech, Revised pourbaix diagrams for zinc at 25–300°C, Corros. Sci. 39 (1997) 107–114, https://doi.org/10.1016/S0010-938X(97)89246-3.
[69] Nuclear Energy Agency (NEA), Chemical Thermodynamics of Iron, Part 1, OECD Publishing, Paris, 2013.
[70] R.J. Lemire, U. Berner, C. Musikas, D.A. Palmer, P. Taylor, O. Tochiyama, Chemical Thermodynamics of Iron. Part 2, OECD Publishing, Paris, 2020.
[71] R.M. Smith, A.E. Martell, NIST critically selected stability constants of metal complexes database, (2004).
[72] P.L. Brown, C. Ekberg, Hydrolysis of Metal Ions, Wiley-VCH Verlag GmbH & Co. KGaA, Weinheim, Germany, 2016.
[73] C.F. Baes, R.E. Mesmer, The Hydrolysis of Cations, John Wiley & Sons, New York, 1977.
[74] D.K. Nordstrom, H.M. May, Aqueous equilibrium data for mononuclear aluminum species, G. Sposito (Ed.). The Environmental Chemistry of Aluminum, CRC Press, Boca Raton, Florida, 1996, pp. 39–80, https://doi.org/10.1201/9780138736781-2.
[75] P. Bénézeth, D.A. Palmer, D.J. Wesolowski, Aqueous high-temperature solubility studies. II. The solubility of boehmite at 0.03 m ionic strength as a function of temperature and pH as determined by in situ measurements, Geochim. Cosmochim. Acta 65 (2001) 2097–2111, https://doi.org/10.1016/S0016-7037(01)00585-3.
[76] Y. Zhang, M. Muhammed, Critical evaluation of thermodynamics of complex formation of metal ions in aqueous solutions, Hydrometallurgy 60 (2001) 215–236, https://doi.org/10.1016/S0304-386X(01)00148-7.
[77] F.J. Mompeán, H. Wanner, The OECD nuclear energy agency thermochemical database project, Radiochim. Acta 91 (2003) 617–622, https://doi.org/10.1524/ract.91.11.617.23468.
[78] OECD Nuclear Energy Agency, Modelling in Aquatic Chemistry, OECD Publications, Paris, 1997.
[79] W. Hummel, Ionic strength corrections and estimation of SIT ion interaction coefficients, Villigen (2009).
[80] Henkel Corporation, Metal Pre-treatment Paves the Way for Greater Sustainability in Automotive Industry, (2022). https://www.henkel-northamerica.com/spotligh

t/2022-13-12-metal-pre-treatment-paves-the-way-for-greater-sustainability-in-automotive-industry-1788088 (accessed March 2, 2024).
[81] M. Pourbaix, Atlas of Electrochemical Equilibria in Aqueous Solutions, 2nd ed., National Association of Corrosion Engineers, Texas, 1974.
[82] C. Vargel, Galvanic corrosion. Corrosion of Aluminium, Elsevier, 2004, pp. 149–164, https://doi.org/10.1016/B978-008044495-6/50013-6.
[83] B. MacDougall, J. Bardwell, M.J. Graham, A Comparison of the passivation of Fe and Ni in borate and sulfate solution, E. MacCafferty, R.J. Broad (Eds.), in: Proceedings of the an International Symposium Honoring Doctor Norman Hackerman on His 75th Birthday, The Electrochemical Society, Pennington, NJ, 1986, pp. 254–266.
[84] S. Thomas, N. Birbilis, M.S. Venkatraman, I.S. Cole, Corrosion of Zinc as a Function of pH, Corrosion 68 (2012) 015009.1–015009.9, https://doi.org/10.5006/1.3676630.
[85] S. Thomas, I.S. Cole, M. Sridhar, N. Birbilis, Revisiting zinc passivation in alkaline solutions, Electrochim. Acta 97 (2013) 192–201, https://doi.org/10.1016/j.electacta.2013.03.008.
[86] R.G. Pearson, Hard and soft acids and bases, J. Am. Chem. Soc. 85 (1963) 3533–3539, https://doi.org/10.1021/ja00905a001.
[87] J.A. Paula, D. Majuste, N.H.J. Freire, E.M. Mazzer, V.F.C. Lins, V.S.T. Ciminelli, Effect of fluoride complexation by aluminium ions on the corrosion behaviour of aluminium cathodes used in zinc electrowinning, J. Mater. Res. Technol. 22 (2023) 2062–2077, https://doi.org/10.1016/j.jmrt.2022.12.037.
[88] G. Shen, L. Chang, C. Jiang, Y. Shao, B. Chen, Effects of F− ions on the electrochemical and interface behavior of cathodes in zinc electrowinning, J. Electroanal. Chem. 939 (2023) 117480, https://doi.org/10.1016/j.jelechem.2023.117480.
[89] T.H. Nguyen, R.T. Foley, On the mechanism of pitting of aluminum, J. Electrochem. Soc. 126 (1979) 1855–1860, https://doi.org/10.1149/1.2128815.
[90] C.J. Brinker, G.W. Scherer, Sol-Gel Science: The Physics and Chemistry of Sol-Gel Processing, 1st ed., Academic Press, Boston, 1990.
[91] G.M. Muha, P.A. Vaughan, Structure of the complex ion in aqueous solutions of zirconyl and hafnyl oxyhalides, J. Chem. Phys. 33 (1960) 194–199, https://doi.org/10.1063/1.1731077.
[92] G. Šekularac, I. Milošev, Electrochemical behavior and self-sealing ability of zirconium conversion coating applied on aluminum alloy 3005 in 0.5 M NaCl solution, J. Electrochem. Soc. 167 (2020) 021509, https://doi.org/10.1149/1945-7111/ab6b0d.
[93] G. Šekularac, J. Kovač, I. Milošev, Prolonged protection, by zirconium conversion coatings, of AlSi7Mg0.3 aluminium alloy in chloride solution, Corros. Sci. 169 (2020) 108615, https://doi.org/10.1016/j.corsci.2020.108615.
[94] L. Li, A.L. Desouza, G.M. Swain, *In situ* pH measurement during the formation of conversion coatings on an aluminum alloy (AA2024), Analyst 138 (2013) 4398–4402, https://doi.org/10.1039/c3an00663h.